Polymeric nanocomposite structure based on functionalized graphene with tunable properties for nervous tissue replacement

A.Talebi [1], S. Labbaf[1*], M. Attari [1], Maryam Parhizkar[2]

[1]Department of Materials Engineering, Isfahan University of Technology, Isfahan, 84156-83111, Iran

[2] School of Pharmacy, University College London, Torrington Place WC1E 7JE, London, UK

*Corresponding author: s.labbaf@iut.ac.ir

Abstract

Electroconductive scaffolds can be a promising approach to repair conductive tissue when natural healing fails. Recently, nerve tissue engineering constructs have been widely investigated due to the challenges in creating a structure with optimized physiochemical and mechanical properties close to the native tissue. The goal of the current study was to fabricate a graphene containing polycaprolactone/ gelatin/ polypyrrole (PCL/ gelatin/ PPy) and polycaprolactone/ polyglycerol-sebacate/ polypyrrole (PCL/PGS/Ppy) with intrinsic electrical properties, through electrospinning process. The effect of graphene on the properties of PCL/gelatin/PPy and PCL/PGS/PPy were investigated. Results demonstrated that graphene incorporation remarkably modulated the physical and mechanical properties of the scaffolds such that the electrical conductivity increased from 0.1 to 3.9 ± 0.3 $S.m^{-1}$ (from 0 wt.% to 3 wt.% graphene) and toughness was found to be 76 MPa (PCL/gelatin/PPy 3 wt.% graphene) and 143.4 MPa (PCL/PGS/PPy 3 wt.% graphene). Also, the elastic moduli of the scaffolds with 0, 1 and 2 wt.% graphene was reported as 210, 300 and 340 kPa in PCL/gelatin/PPy system and 72, 85 and 92 kPa for PCL/PGS/PPy system. Cell viability study demonstrated the non-cytotoxic nature of the resultant scaffolds. The sum of results presented in this study suggest that both PCL/gelatin/PPy/graphene and PCL/PGS/PPy/graphene compositions could be a promising biomaterial for a range of conductive tissue replacement or regeneration applications.

Keywords: Conductive Scaffold; Nanofiber; Polycaprolactone; Gelatin; Polyglycerol-sebacate; Graphene; Nerve tissue engineering.

Introduction

The nervous system is considered as one of the most complex human tissue owed to its unique electrical, mechanical and chemical nature. The therapy and regeneration of the nervous tissue is very much reliant upon the type, size and severity of the injury. Typically, autologous grafts are the first choice of medical approach in nerve reconstruction and is widely applied to treat neural defects [1,2]. However, autografts have limitations that include shortage of nerve supply, lack of functional recovery and the possibility of neuroma formation [3]. Therefore a fundamental strategy would be to create a simulated functional and electrically conductive graft to enhance nerve regeneration for the replacement of injured tissue [4].

Creation of an optimized scaffold that is bio-functional still remains a challenge. Fibrous scaffolds provide a platform for cell proliferation and attachment because they resemblance the natural extracellular matrix. Fabrication techniques such as electrospinning enables the creation of structures that closely mimic the unique properties of the native tissues. Through electrospining, a range of properties for the resultant structure can be easily tuned by modifying the process parameters and the material selection.

Polymer blending is one of the most applicable methods in developing novel and appropriate composites for specific applications like biosensors [5,6], hydrogels [7,8] and drug delivery systems [9] in various tissues [10,11]. Scaffolds based on blend of synthetic and natural polymer have shown improvement in cell adhesion and biodegradation [12–14]. Nonetheless, the nerve grafts created using the aforementioned polymers, under long repeated mechanical stress, have mostly resulted in inelastic deformation and mechanical failure [15]. Hence, to overcome

these drawbacks, there is currently a great need for the development of an elastomeric structure with suitable chemical, mechanical and biodegradation properties.

Poly glycerol-sebacate (PGS) is a biodegradable, biocompatible and non-cytotoxic elastomer, that has been commonly applied in numerous applications such as nerve grafts and cardiovascular systems [16,17]. However, the majority of the reported studies presented limitations like complicity in production process, incapability to manage the properties of the structures, limited fiber diameter and incontrollable biodegradation rate [18,19]. Therefore, it is suggested to blend a fairly strong biopolymer such as polycaprolactone (PCL) with an elastomeric polymer (PGS) to develop a biomaterial with tunable mechanical, electrical and chemical properties suitable as nerve graft. PCL is a semi crystalline linear hydrophobic polymer. While the electrospun PCL scaffolds could mimic the uniqueness of ECM architecture and morphology and provide the toughness that is needed in a native tissue, its poor wettability can cause a decrease in cell adhesion, proliferation, movement, and differentiation [20,21]. To overcome these limitations, it is suggested to blend PCL with a natural polymer. Gelatin is a natural collagen derived biopolymer with high hydrophilicity which is extensively applied for tissue engineering purposes [21,22]. The electrical and mechanical properties are considered as a key characteristics crucial for a nerve tissue engineering applications [23,24].

In order to provide electrical simulation suitable for nerve conduits, various materials have previously been evaluated including, but not limited to, poly lactic acid (PLA):carbon nanotube micro fibrous scaffolds [25], chitosan/PCL fibrous mat [26] and poly (3, 4-ethylenedioxythiophene):chitosan/gelatin fibrous structures [27]. However, the majority of the above-mentioned scaffolds show some drawbacks such as low conductivity and the inability

to mimic the native tissue. In our previous studies [28,29], PCL containing bio-composite constructs were used to mimic the native cardiac tissue through the optimization of electrical conductivity (5 $S.cm^{-1}$) and mechanical stiffness (100 KPa). The findings were based on the effect of polypyrrole (PPy) and graphene incorporation within the PCL structure. Combination of PPy and graphene can provide the electrical conductivity that is necessary for nerve tissue therapy. It is worth mentioning that the carbocyclic group on functionalized graphene could support the intermolecular interaction in polymeric structure as well as nurturing a more biocompatible structure for cell regeneration. Nevertheless, there are no information on PCL/gelatin/Polypyrrole/graphene and PCL/PGS/PPy/graphene nano-fibrous scaffolds for nerve tissue applications. It is hypothesized that the mechanical properties and hydrophobicity will be greatly influenced by the presence of gelatin and PGS in the polymeric network. Hence, the current study focuses on the utilization of electrical components to create a conductive construct with properties suitable for nerve tissue repair applications.

Experimental Section

2.1 Materials

PCL (Mn 80,000), gelatin (Mn 50,000), Pyrrole, glycerol and sebacic acid were obtained from Sigma–Aldrich; multilayered graphene nanosheets (thickness smaller than 40 nm and lateral size 1μm) were purchased from VCN materials. $FeCl_3$, Chloroacetic acid, Sodium hydroxide, para toluene sulfonate(pTS), acetic acid and formic acid were obtained from Merck Co.

2.2 Polymerization of PGS

A volume of glycerol and sebacic acid with 1:1 M ratio was mixed at 120 °C under nitrogen atmosphere and extreme vacuum (less than 50 mTorr) for a day to produce PGS prepolymer [30]. The crosslinking density is 38.3 ± 3.40 mol/m3, and relative molecular mass between crosslinks is 18,300 ± 1,620 for PGS prepolymer.

2.3 Polypyrrole polymerization

All the chemical syntheses reactions were done in deionized ultrapure water at 5 °C[31]. Oxidizing agent ($FeCl_3$) and pTS (dopant) solutions (0.1 M) were used to polymerize polypyrrole (PPy) with chemical method then pyrrole suspension (0.1 M) was mixed with a pTS (dopant) solution with the same ratio (monomer: dopant,1:1). Following, ferric chloride (oxidizing agent) was gently added to the system with the ratio of 1:2.4 (monomer: oxidant) under low stirring rate for 30 minutes [32]. Polymerization reaction was continued for four hours under constant stirring; the polymerized pyrrole was then centrifuged, washed and dried.

2.4 Chemical functionalization of graphene by carboxyl group

2.57 g of Sodium hydroxide tablet with 1.2 g of chloroacetic acid powder was dissolved in 1 ml of Graphene suspension (1M) in deionized ultrapure water and mixed for 5 minutes to solve all powders. Then, the solution was left under ultra-sonication (sonication power was 500 watt) for 3 hours to complete the reaction [33]. Chemical functionalization of graphene by carboxyl group showed in following equation.

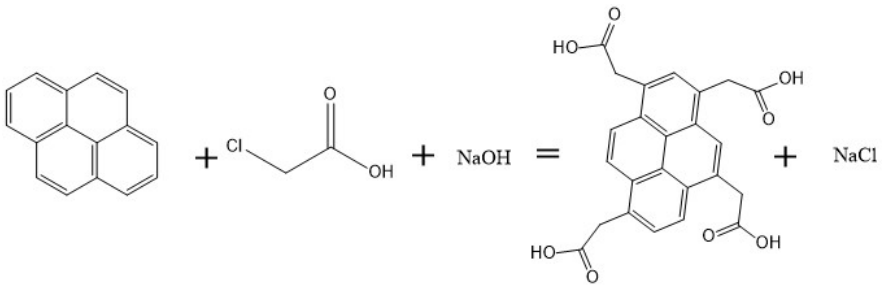

Graphene nano sheet Chloroacetic acid carboxyl functionalized graphene

2.5 Fabrication of fibrous scaffolds

All polymeric solutions were prepared based on Table 1. The multilayered functionalized graphene powder was scattered in formic acid/ acetic acid (ratio of 7:3) solvent by ultra-sonication. Subsequently, the graphene solution was added to the polycaprolactone/gelatin/polypyrrole and polycaprolactone/Polyglycerol-sebacate/polypyrrole blend and stirred for three hours until complete homogeneous solution was prepared. Electrospinning process was optimized by using a 21G needle under 10 ± 2 kV high voltage with the infuse rate of 2 ml per hour. The Electrospinning process was performed at 25 ± 3 °C and a humidity of 40 ± 6%. 15 cm gap was fixed between the collector and needle.

Table1. Concentration of each sample in 30% acetic acid/ 70%formic acid solvent.

SAMPLES		PCL (wt.%)	Gelatin (wt.%)	PGS (wt.%)	PPy (wt.%)	Graphene (wt.%)	Electrical conductivity of Polymer solution (mS)	Viscosity of Polymer solution (cP)
PCL/ GRAPHENE /PPY	PG0 (without Graphene)	4.36	-	1.86	0.49	-	2.45 ± 0.06	196 ± 6
	PG1 (Graphene (1%))	4.36	-	1.86	0.49	0.032	2.91 ± 0.06	222 ± 5
	PG2 (Graphene (2%))	4.36	-	1.86	0.49	0.098	3.74 ± 0.05	241 ± 8
	PG3 (Graphene (3%))	4.36	-	1.86	0.49	0.164	4.42 ± 0.07	300 ± 9
PCL/ GRAPHENE /PPY	GG0 (without Graphene)	4.36	1.86	-	0.49	-	2.23 ± 0.04	189 ± 8
	GG1 (Graphene (1%))	4.36	1.86	-	0.49	0.032	2.85 ± 0.05	214 ± 7

	GG2 (Graphene (2%))	4.36	1.86	-	0.49	0.098	3.64 ± 0.06	232 ± 9
	GG3 (Graphene (3%))	4.36	1.86	-	0.49	0.164	4.28 ± 0.05	278 ± 11

2.6 Characterizations

Chemical testing: Fourier Transform Infrared Spectroscopy FTIR (Bruker tensor) was used in the range of 400-4000 cm^{-1} to detect the structural characteristics of the polymeric structures.

Surface morphology: Scanning Electron Microscopy (SEM, Philips) was used to inspect diameter and morphology of the electrospun nanofibrous sheets. For better vision, SEM samples were covered with thin layer of gold (6 μm). The norm fiber size (n=50) was measured using Digimizer software to process SEM images.

Wettability testing: A optical contact angle measuring device was operated for wettability evaluations. To achieve consistency, identical pictures of the surface 3 × 1 cm samples were fixed on a thin flat piece of glass and 6 μL droplet of deionized water was used for the test. Both sides of the drop were measured to establish the contact angle (n=6).

Mechanical testing: Straps of nanofibrous scaffolds (4 × 1 cm) were used to investigating the mechanical factors by Tensile testing (Hounsfield H25KS). For wet state testing, samples were immersed and soaked in the buffer solution (PBS) and prepared for the test. For each condition at least 3 samples were measured.

Electrical Conductivity: 10×30 mm^2 straps of nanofibrous scaffolds were used to measure the electrical conductivity. Gold-coated probes were used to measure conductivity by two

contact method (Instek LCR-819 High Precision LCR Meter), at 25 ± 2 °C. The Conductivity ($C_{(S.cm^{-1})}$) of the samples was determined as below:

$$C = \frac{L}{R \times w \times t}$$

Here, L is the length (cm) of the sample, and W is the width (cm) of the sample, and t is the thickness (cm) of the sample and R is the resistance (Ω) of samples evaluated by LCR Meter.

2.7 Degradation

Biodegradation of samples were studied for four weeks. To perform the test, samples were added to phosphate-buffered solution (PBS, pH 7.4) with a ratio of 0.01g: 5 ml and then retained at 37 °C. At each time point (1, 3, 5, 7, 14, 21 and 28 days), the buffered solution was removed and samples rinsed in deionized water to dissolve the adsorbed salts. Next, samples dried and re-weighed to establish the change in dry mass after incubation periods. Degradation (D) was computed using the following formula:

$$D\% = \frac{\boldsymbol{Wi} - \boldsymbol{Wt}}{Wi} \times 100$$

Here, W_i is the initial dry weight of the patch, and W_t is the dry weight after time t.

2.8 Hemocompatibility

Platelet adhesion: To evaluate the blood related assay, human blood was taken from a healthy adult volunteer with informed consent under regulations of Isfahan University of Technology. Measurement of lactate dehydrogenase (LDH) appear after lysis of the adhered platelets was used to establish the platelet adhesion. Test was done by centrifuging 30 ml of

fresh human complete blood at 2000 RPM for 20 min to prepare platelet rich plasma (PRP) from blood [30]. Human fresh platelet rich plasma (PRP) was added to the samples and placed in a 48 well plate and ePTFE and glass samples was used as a positive and negative controls, respectively. Then samples were placed in an incubator at 37 °C for 120 minutes. Next, PRP was removed, and samples were rinsed several times with PBS to ensure the elimination of unattached platelets. Half of the samples were immersed in 2.5 wt% glutaraldehyde solution for 45 minutes at the room temperature, then washed and air-dried overnight. The platelet adhesion was studied on the surface of the samples by SEM. The other half of samples was treated with 40 µL of Triton X-100 (Sigma Aldrich, diluted to 1%) at 37°C for 30 minutes to cause cell lysis and releasing of LDH. Then 20 µL of each lysate solution added to 1 mL of a substratum solution including pyruvate and NADH. LDH catalyzes the decrease of pyruvate by NADH. The absorbance was measured at 60 seconds intervals till 180 seconds. The LDH concentration in the sample was calculated by the following equation:

$$\text{LDH concentration(U/L)} = \frac{\Delta A}{\text{min}} \times \frac{(V_t \times 10^6)}{\varepsilon \times V_s}$$

where ΔA/min is the average of absorbance data; the molar absorbance of NADH at 340 nm is ε; Vt is total reaction volume; and Vs is the sample volume.

Red blood cells hemolysis: Previously separated red blood cells (RBCs) from blood plasma, were thinned in physiological solution for more accurate measurements. Next, scaffolds immersed in the thinned red blood cells solution at 37 °C for 60 minutes. Moreover, distilled water and physiologic serum were used as positive and negative controls. To measure the hemolysis ratio, liquid from each sample was centrifuged after incubation period and

examined at 542 nm by UV-vis spectrometer. The hemolysis ratio was evaluated as below (equation 8):

$$\text{RBCs hemolysis \%} = \frac{I_S - I_N}{I_P - I_N} \times 100$$

where, I_S (each samples), I_N (negative control) and I_P (positive control) represent the UV-vis intensity.

Blood Coagulation: Whole blood kinetic clothing time method was used to established the thrombogenicity of the samples. Glass and ePTFE samples used as the positive and negative controls samples. 500 µL of $CaCl_2$ was mixed to 5 mL of anticoagulant whole blood, and samples was incubated with 100 µL of the activated blood. All of the samples placed in individual 12-well plate for 5, 15, 25, 35 and 45 minutes at room temperature. 2.5 mL of deionized water was added to the samples at the end of each time point. The suspension was distributed into a 96-well plate, and the released hemoglobin from red blood cells that been lysed was measured at 542 nm by spectrophotometric plate reader (BioTek, FLX800). The absorbance of the clotted red blood cells was drawn versus the blood treatment time.

2.9 Biological Evaluations

Electrospun Fibers were prepared according to parameters in section 2.4 and was collected on circular cover slips suitable for a 24-well plate. UV sterilization was conducted to eliminate contamination. Human fibroblast cells (Royan ATMP-HDFs cell line) were maintained in a 50 cm^3 tissue culture flasks at 37 °C in a humidified 5 % CO_2 atmosphere in an incubator, in RPMA1640 culture media (Gibco, Germany) with 10 % FBS (fetal bovine serum) (Gibco, Germany).

To evaluate the toxicity of the scaffolds, MTS viability rest was conducted according to manufacturer's method. In this regard, a seeding density of 30,000 cells/well was selected. The mitochondrial activity of the cultured cells was controlled using a colorimetric MTT (3-[4,5-dimethylthiazol-2yl]-2,5-diphenyl tetrazolium bromide) assay. At the end of each time point, the absorbance was read at 540 nm by ELISA reader (Awareness Technology INC.). Here, for better comparison, two control groups of positive (cells only) and negative (cells with DMSO) was used.

For cell attachment study, after 72 h of culture, the cell seeded onto the scaffolds were washed with PBS (pH 7.4) and placed in 4.5 % glutaraldehyde for 3 h to enable cell fixation. Then, scaffolds were washed with PBS followed by a course of dehydration procedure using ethanol (from 60 to 100 %) and then dried for 24 h. For SEM visualization, the scaffolds were sputter coated with a gold layer prior to imaging (SEM, Philips).

2.10 Statistical analysis

statistical evaluations were done by One-way ANOVA. To investigate significant variances between results, Tukey's post-hoc test used by Prism Software (V.8). P-value <0.05 was measured significant.

3 Results and discussion

3.1 Physical properties

Nanofibrous scaffolds, with different ratios of graphene nanosheets, were fabricated through electrospinning technique. Fig. 1(A-H) shows the effect of various ratios of graphene on the diameters and morphology of the resultant nanofibrous structure. The surface morphology of

the electrospun defect-free PCL/gelatin/PPy/graphene nanofibers with 1 and 3 wt.% graphene shows an average diameter of 350±52 and 90 ± 34 nm, respectively while in PCL/PGS/Ppy/graphene scaffolds the fiber diameter appears to slowly reduce in a pattern of PG0 > PG1 > PG2> PG3 from 250 nm in PG0 to 200 nm in PG3. Hence, it is apparent that with the increase in graphene nanosheet, the average diameter reduces significantly. This may be caused by the enhanced electrical conduction of the spinning dope that could help the polymeric stream to form finer fibers during fabrication. The high electrical conduction of the polymeric solution generates a more powerful electrical force during the spinning course preceding to superior strain and smaller fiber diameter [34]. Also adding graphene nanosheet produces a more viscous mixture that results in finer fibers (Table 1). This is in accordance to our previous findings [32].

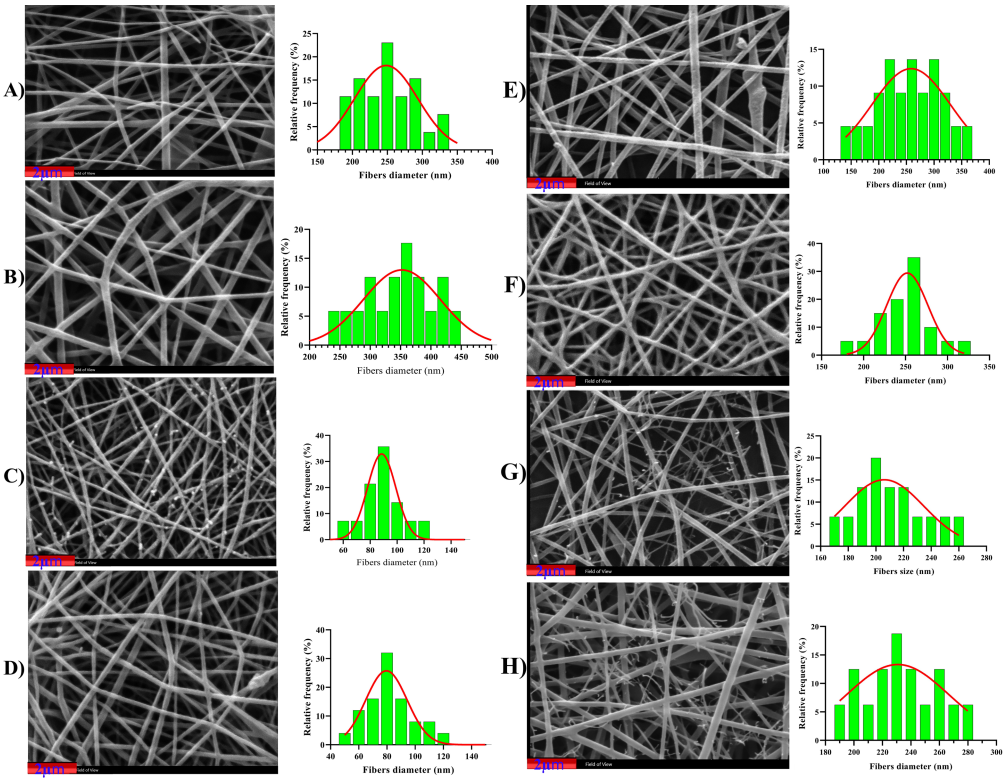

Figure 1. SEM images and fiber diameter size distribution for PCL/gelatin/PPy/graphene system with A) 0 wt.% B) 1 wt.% C) 2 wt.% D) 3 wt.% graphene incorporation and for PCL/PGS/PPy/Graphene system E) 0 wt.% g F) 1 wt.% G) 2 wt.% and H) 3 wt.% graphene. (Scale bar: 2 μm)

Wettability results demonstrate that the PCL/gelatin/PPy scaffold with a contact angle of 79.5° ± 2. 1° is hydrophilic (Fig. 2A). Functionalized graphene with carboxylic groups contributes towards the hydrophilicity of the samples. With the increase in graphene ratio from 1 to 3 wt.% in the PCL/ gelatin/ PPy/ graphene nanofibers, a decreased from 63.4° ± 2. 7° to 41.7° ± 2. 7° is evident in water contact angle results.

Furthermore, with increase in graphene concentration, the hydrophilicity is also improved in PCL/PGS/Ppy/graphene nanofibers such that in PG3 sample contact angle of 31.7° ± 2 compared to 51.4° ± 3 in the control group PCL/PGS/PPy fibers is detected. Also, water drops on PG1, PG2 and PG3 were absorbed within 5 to 10 seconds demonstrating their high wettability, which is considered an important characteristic for cell support and attachment.

Based on our previous study [28], it was found that the electrical conductivity of the scaffolds were influence by the concentrations of polypyrrole (PPy) as a result of conductive network throughout the polymeric chains that act as a linker between graphene nanosheets. This phenomenon enhances the electron current velocity throughout the network. In the current study, the conductivity was tuned by controlling graphene concentration (Fig. 2B). Samples show a conductivity of 1.7 ± 0.2 $S.m^{-1}$ (1 wt.% graphene), 3.1 ± 0.3 $S.m^{-1}$ (2 wt.% graphene) and 3.9 ± 0.3 $S.m^{-1}$ (3 wt.% graphene) in wet condition for PCL/gelatin/PPy/graphene nanofibers. Also, in PCL/PGS/Ppy/graphene nanofibers the conductivity of the fibrous mats shows an increase from 1.1 ± 0.2 $S.m^{-1}$ to 3.9 ± 0.2 $S.m^{-1}$ as the graphene content increases

from 0 wt.% to 3 wt.%. As expected, the electrical conductivity was improved by an increase in graphene concentration. Established results are in the general reach of electrical conduction that is reported for native neural tissue [35]. Also, compared to similar attempts in creating fibrous platform for nerve tissue regeneration, this system showed a superior electrical conductivity [36]. For example, Baniasadi et al.[37] fabricated a conductive scaffold by incorporating polyaniline/graphene (PAG) nanoparticles into a chitosan/gelatin matrix with 0.1 $S.m^{-1}$ conductivity. In a different study Zhou et al.[38] developed polypyrrole/poly(lactic acid) nanofibers to regenerate peripheral nerve with a 1×10^{-4} $S.cm^{-1}$ electrical conductivity. Also Soltani *et al*.[39] formulated a conductive scaffold containing graphene with 3.3 $mS.cm^{-1}$ in film form.

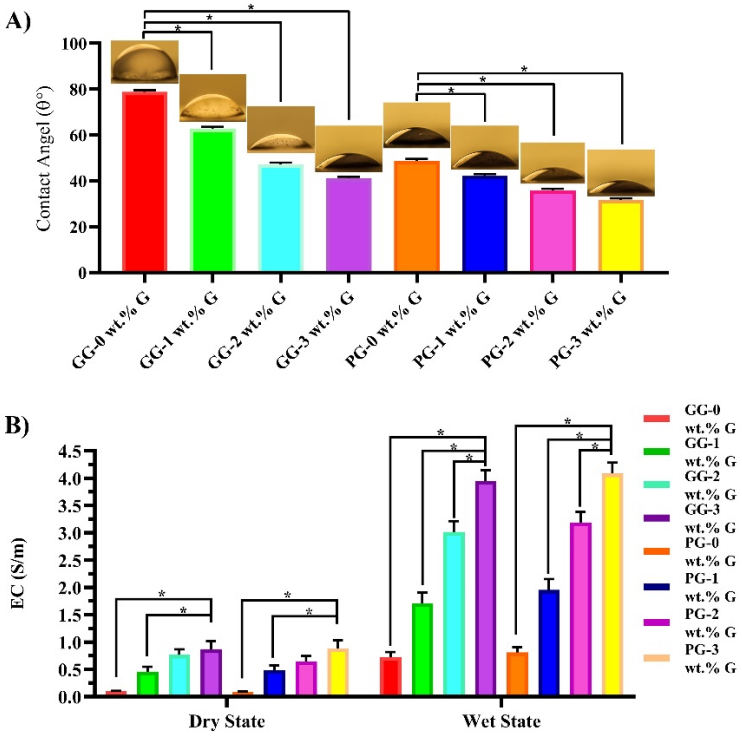

Figure 2. A) Images of water contact angle and average water contact angles of the of fiber mats. B) Electrical conductivity of fiber mats. Error bars indicate standard error of the means, asterisks mark significance levels of $p < 0.05$ (*).

3.2 Chemical Evaluations

Fig. 3 presents the FTIR spectra for PCL/gelatin/PPy/graphene and PCL/PGS/PPy/graphene scaffolds. Commonly, PCL is marked with asymmetric $-CH_2$ stretching at 2973 cm^{-1}, symmetric $-CH_2$ stretching at 2842 cm^{-1}, ester group at 1777 cm^{-1} where the normal bands of C=O stretching at 1675 cm^{-1} (amid I), and N–H bending coupled with C–N stretching at 1556 cm^{-1} (amide II) and asymmetric C-O-C stretching at 1239 cm^{-1} for gelatin structure[28]. In PCL/PGS/PPy/graphene scaffolds energy band slightly changed in a way that PCL bands with asymmetric $-CH_2$ stretching at 2969 cm^{-1}, symmetric $-CH_2$ stretching at 2813 cm^{-1}, ester group at 1789cm^{-1} are detected. The common bands for PGS carbonyl stretching at 1778 cm^{-1}, C=O stretching at 1358 cm^{-1} (amid I), and N–H bending coupled with amide II C–N stretching at 1256 cm^{-1}. Moreover, the stretching of C–O and C-C stretching is also noticed in the range of 1000–1250 cm^{-1} and asymmetric C-O-C stretching at 1079 cm^{-1}. Also, the interaction of carboxyl groups on the functionalized graphene with polymers structures and amide groups in gelatin chain and polypyrrole ring can lead to the development of a new covalent intermolecular bond [29]. Besides, expected intermolecular hydrogen bonds between polymeric structures are presented in Fig. 4. This interaction is inveterate through the changing of the distinctive bands of polymer chain (i.e., amide I and amide II) to lesser wavenumbers alongside with lowered intensity diffraction in the FTIR spectra curves (Fig. 3) in both polymeric systems.

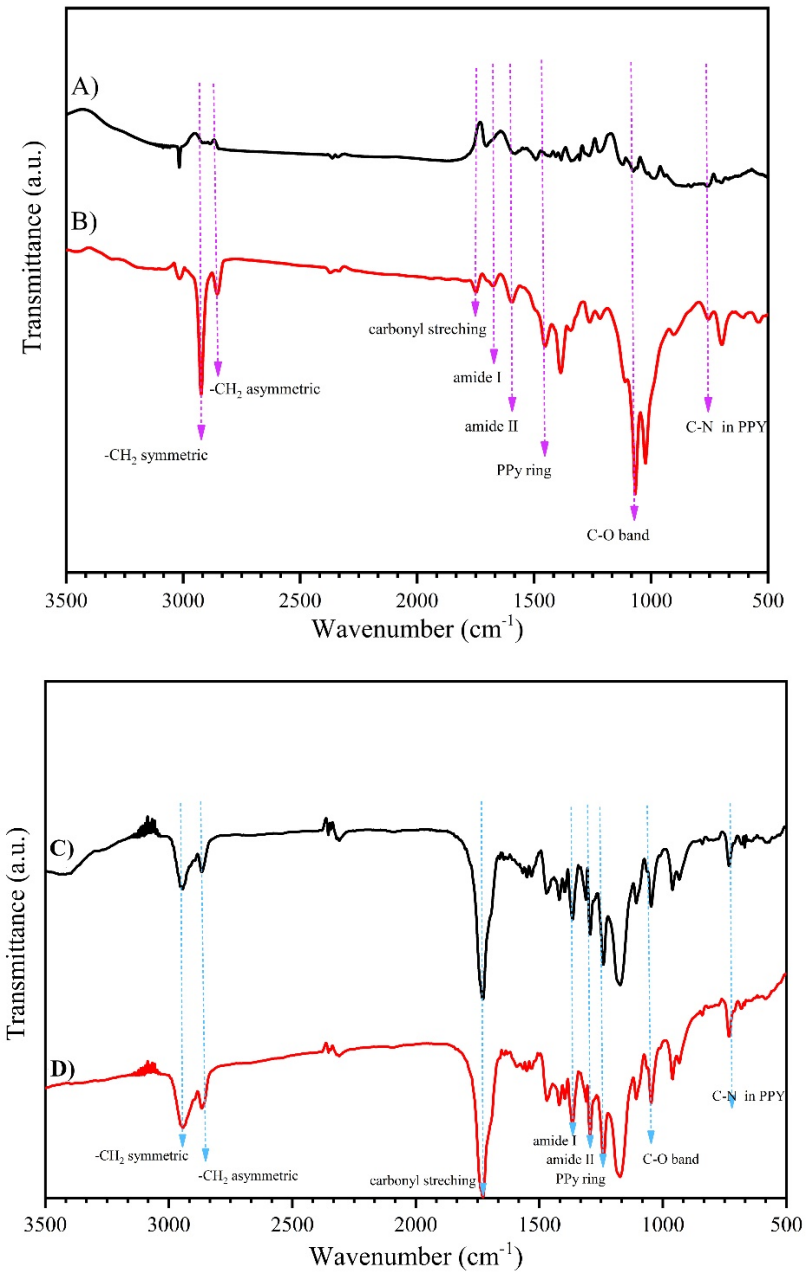

Figure 3: FTIR characterization of nanofibers for A) PCL/gelatin/PPy/graphene B) PCL/gelatin/PPy C) PCL/PGS/PPy/Graphene and D) PCL/PGS/PPy.

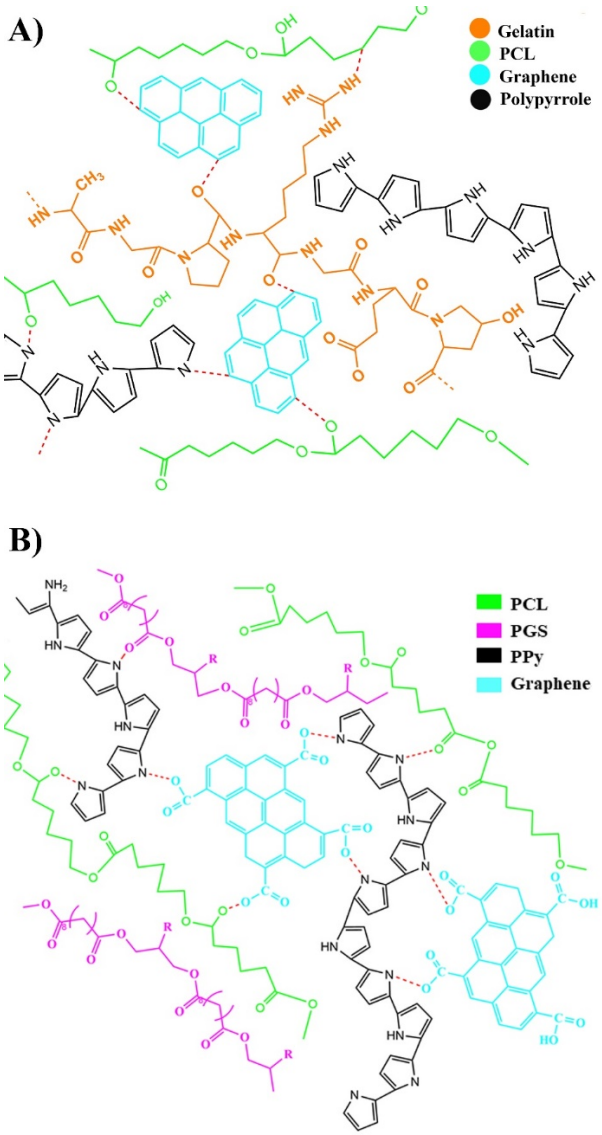

Figure 4: Schematic illustrations of the interaction between the composite components in A) PCL/gelatin/PPy/graphene system B) PCL/PGS/PPy/graphene system.

3.3 Nanocomposite mechanical properties

The stress–strain curve for the nanofibrous PCL/gelatin/PPy/graphene and PCL/PGS/PPy/graphene scaffolds are presented in Fig. 5. The blending of graphene with PCL/gelatin/PPy and PCL/PGS/PPy has significantly enhanced the mechanical behavior of the composite structure. The strain for the samples with graphene was improved by 76% in comparison to the PCL/gelatin/PPy sample (Table 2) which may be due to the intermolecular

bands in the polymeric network (Fig. 4). The tensile strength (2.71 MPa) of the PCL/gelatin/PPy/3 wt.% graphene (GG3) nanofiber mat showed a 46 % improvement, compared to the sample without graphene (GG0) (1.85 MPa) scaffold. The tensile strength (2.66 MPa) of PCL/PGS/PPy/3 wt.% graphene (PG3) nanofiber reached 52 % improvement compared to PG0 (1.75 MPa) group. All fibrous scaffolds demonstrated a good toughness such that for without graphene (GG0) sample 28 MPa, (PG0) 42 MPa and for 3wt.% graphene (GG3) sample up to 76 MPa, 143 MPa for PG3, revealing more than 230% increase in PCL/gelatin/PPy system and remarkable 330% increase in PCL/PGS/PPy system. These polymeric system offers highly tunable deformability (up to 67 MPa toughness for GG3 and 143 MPa for PG3), flexibility (up to around 75% elongation for both systems) and strength (up to 1.31 MPa in GG0 and 1.5 MPa in PG0 tensile strength in wet state). For example, the elastic steep of PCL/gelatin/PPy with 0, 1 and 2 wt.% Graphene was 210, 300 and 340 kPa and for PCL/PGS/PPy with 1, 2 and 3 wt.% Graphene was 85, 92 and 97 kPa, respectively. These values are within the range of the stiffness stated for the natural spinal cord and peripheral nerve system tissue (~20-350 kPa) [40–42] and other connective tissue such as natural myocardium (~ 30-100 kPa) [43].

The Tensile strength in PCL/gelatin/PPy with 1-3 wt% graphene in the system is 1.85, 2.24, 2.71 MPa, respectively. However, in 3 wt.% graphene samples the strength had reduced to 2.38 MPa, whilst elongation and toughness also decreased due to the increased probability of agglomeration that could potentially affect the mechanical properties. Also, in PCL/PGS/PPy system the same trend could be observed. Elongation intends to improve in wet condition due to the swelling of the fibers, which change the diameter, twisting angle and lowers the friction coefficient of the fibers [44]. Hence, the strong decrease in friction influences the

reduction in the modulus and tensile strength. Plus, the strain at break was increased (78% in GG3 and 75% in PG3) because of the high modulus area points to the fiber original movement and the low modulus area mostly alter on the fiber aligning and slippage. In the wet condition, initial mobility of the fibers reduces due to the decrease of the friction coefficient between fibers and enlarges the fibers' stretching phase which lets the fibers to straighten out without breaking and shredding, and growing in length, which is the key cause for their strain increase in a wet state.

All the mechanical properties in wet condition were measured to be lower than the dry condition in both systems. This could be due to fibers swelling ratio and lower friction factor which could promote the elongation in wet condition test. Although, the mechanical properties were less favorable in the wet condition, they were still tolerable for supporting native tissue.

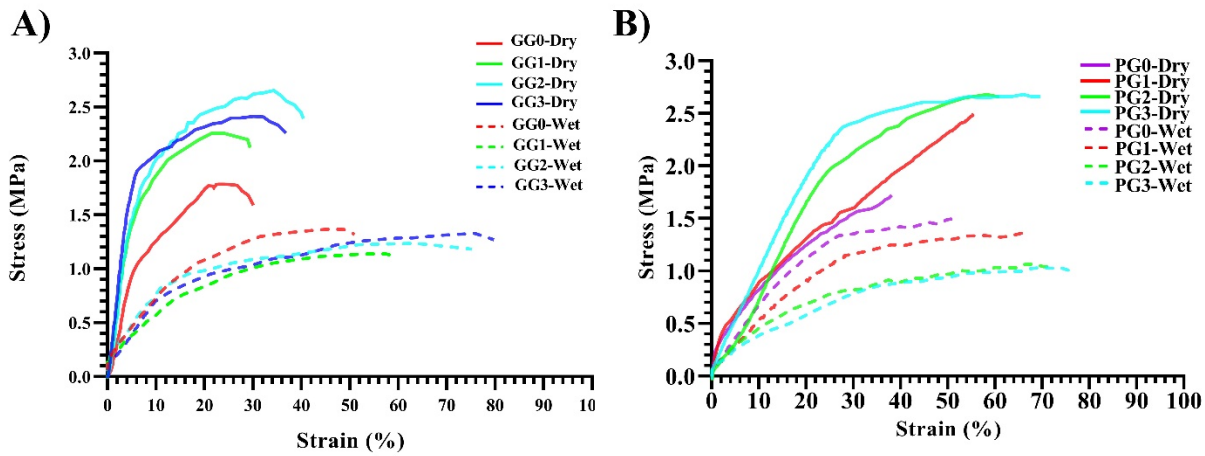

Figure 5: Stress-strain; diagram of A) PCL/gelatin/PPy/graphene system B) PCL/PGS/PPy/graphene system (significance levels of $p < 0.05$ (*) and $p < 0.01$ (**)).

Table 2: Mechanical properties of scaffolds in dry and wet conditions.

Sample	Tensile strength (MPa)		Tensile modulus (KPa)		Elongation (%)		Toughness (MPa)	
	Dry	Wet	Dry	Wet	Dry	Wet	Dry	Wet
GGO	1.85 ± 0.2	1.31 ± 0.1	210 ± 13	56 ± 2	22 ± 2	49 ± 4	28.34 ± 3.2	46.29 ± 4.2
GG1	2.24 ± 0.3	1.08 ± 0.2	300 ± 14	43 ± 1	26 ± 3	58 ± 3	42.89 ± 3.5	41.34 ± 3.9
GG2	2.71 ± 0.2	1.21 ± 0.2	340 ± 21	61 ± 2	36 ± 2	67 ± 4	76.27 ± 4.8	60.71 ± 4.5
GG3	2.38 ± 0.4	1.31 ± 0.2	370 ± 23	63 ± 3	32 ± 3	78 ± 2	67.11 ± 5.1	76.84 ± 9.1
PG0	1.75 ± 0.3	1.5 ± 0.1	72 ± 3	65 ± 2	38 ± 2	51 ± 3	42.85 ± 2.2	56.29 ± 3.2
PG1	2.49 ± 0.3	1.3 ± 0.2	85 ± 4	49 ± 1	54 ± 4	65 ± 2	83.89 ± 4.5	66.31 ± 3.4
PG2	2.65 ± 0.1	1.11 ± 0.1	92 ± 6	48 ± 2	59 ± 3	71 ± 4	110.5 ± 5.8	56.7 ± 3.7
PG3	2.66 ± 0.2	1.01 ± 0.2	97 ± 3	37 ± 3	68 ± 3	75 ± 2	143.4 ± 6.9	56.99 ± 5.1

Significance levels of $p < 0.05$ (*) and $p < 0.01$ (**)

3.4 Biodegradation study

The physical properties of the scaffolds can be affected by additional water consumption [45]. Hence, it is important to investigate the changes in polymeric behavior following immersion in biological fluids. The degradation of PCL/gelatin/PPy/graphene and PCL/PGS/PPy/graphene scaffolds in PBS was observed over 28 days' period (Fig. 6). Biodegradation of the scaffolds were altered alongside with the topographical factors and chemical alignment of the polymeric scaffolds. The result of sample degradation presents a semi-linear profile for both systems. The data of PCL/gelatin/PPy/graphene scaffolds show a higher degradation ratio. The observed difference between various groups could be due to the amine groups, hydroxyl and carboxylic on the activated graphene and gelatin that can enhance biodegradation. Besides, the ester bonds of sebacic acid and glycerol monomers in

PGS network may control the degradation rate of the scaffolds [46,47]. As well as chemical factors, topographical conditions such as fibers diameter of the mats are effective to the degradation profile. The finer fiber diameter of the graphene contained scaffolds could accelerate the hydrolysis alongside weight loss compared to the thicker nanofibrous scaffolds due to enhanced contact area. Based on the properties evaluated for all groups containing various amounts of graphene, the 3 wt.% graphene scaffolds in both systems were found to be the optimum structure due to its great mechanical strength, elongation, superior electrical conductivity and wettability, hence, taken forward for the blood compatibility evaluation and cell studies.

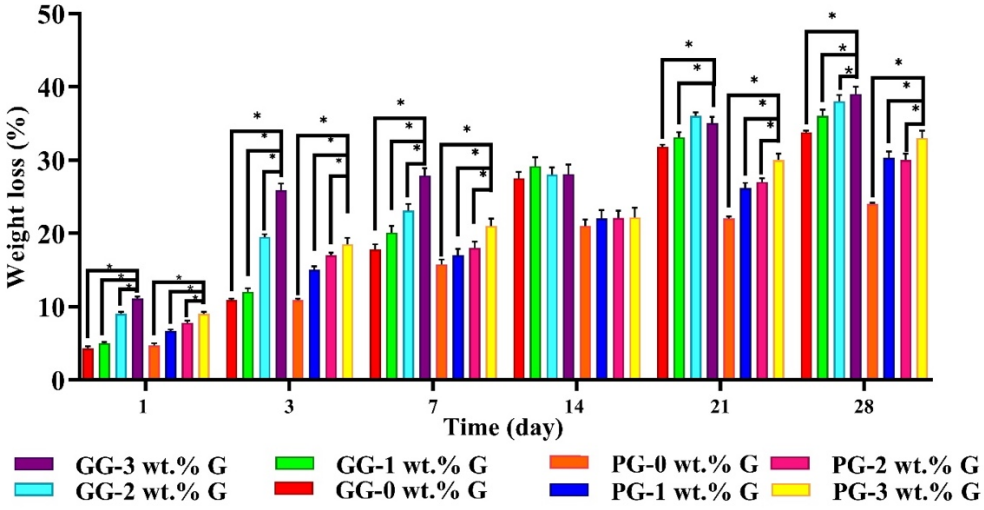

Figure 6: Weight loss of different concentrations of both systems after incubation in PBS solutions for various periods (pH: 7.4). Error bars indicate standard error of the means, asterisks mark significance levels of $p < 0.05$ (*).

3.5 Hemocompatibility study

The blood compatibility evaluation is essential for confirming the suitability of a device for blood-contacting applications. Surface properties of the biomaterials trigger platelets to attach

on to the surface of a foreign material and they can become activated to preform blood coagulation and thrombosis [48]. Hence, the hemocompatibility of blood-contacting materials is a vital factor for numerous practical applications [49]. In this study, blood compatibility of PCL/gelatin/PPy/graphene scaffolds prepared using 3 wt.% graphene was evaluated by studying the platelet adhesion, red blood cells (RBC) hemolysis and blood coagulation of scaffolds.

LDH activity has a direct relation with the number of adhered platelets on the surface area of a material. As shown in Fig. 7A, LDH concentration for samples were found to be 21 ± 5, 19 ± 4, 22 ± 6, and 274 ± 14 $U.L^{-1}$ in response to PCL/gelatin/PPy/graphene scaffold, PCL/PGS/PPy/graphene scaffold, ePTFE, and glass samples, respectively. Fig. 7B shows SEM images of platelet adhered on the surface of scaffold. As it appears, none of the attached platelets are pseudopodium or aggregated and activation process not occurred for any of platelet. These results suggest the great capability of electrospun PCL/gelatin/PPy/graphene scaffolds and PCL/PGS/PPy/graphene scaffold in slowing down the platelet adhesion compared to glass samples.

Hemolysis ratio is an important factor for evaluating compatibility with blood [50]. The ratio of hemolysis represents the release of hemoglobin that is initiated by ruptured red blood cell. In the time that samples are in contact with RBC, samples could initiate the inner and outer membrane degradation of red blood cells, hence start to hemolysis [51]. The hemolysis ratios for PCL/gelatin/PPy/graphene scaffold, PCL/PGS/PPy/graphene scaffold, negative and positive controls sample are shown in Fig. 7B. The tested scaffold showed a low hemolysis ratio of 2.3% for PCL/gelatin/PPy/graphene scaffold and 2.1% for PCL/PGS/PPy/graphene scaffold which is significant different to glass sample (5.7%) and a previous report [52]. All the

medical materials with hemolysis ratio below 5%, are accepted as non-hemolytic as stated by international biological safety association [53], so PCL/gelatin/PPy/graphene scaffold and PCL/PGS/PPy/graphene scaffold are hemocompatible.

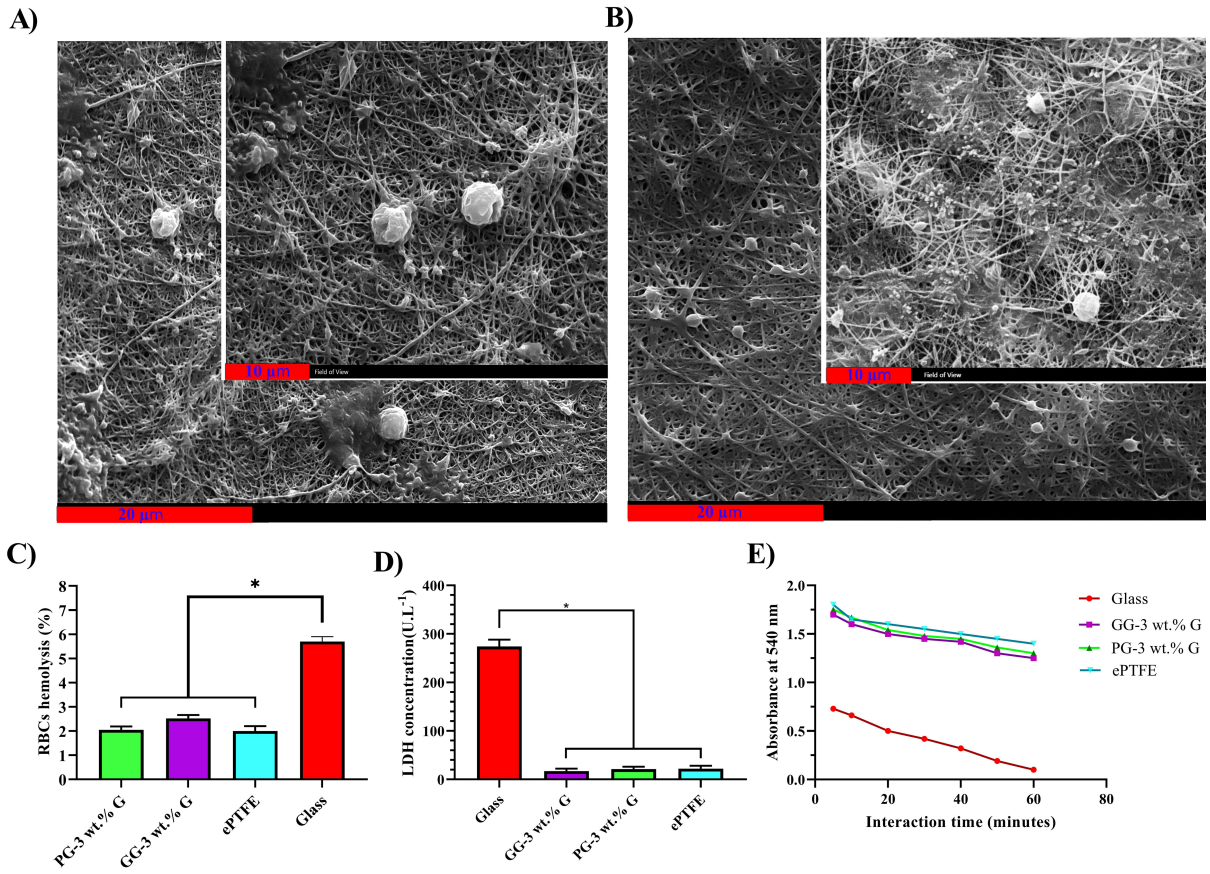

Figure. 7: A-B) SEM images of platelet adhered on the surface PCL/gelatin/PPy/graphene (A) and PCL/PGS/PPy/graphene (B) system. C) red blood cells hemolysis, D) LDH concentration and e) blood coagulation profile. Error bars indicate standard error of the means, asterisks mark significance levels of $p < 0.05$ (*). (Scale bar: 20 µm and inner scale bar: 10 µm).

Fig. 7D denotes the blood coagulation data for nanofibrous PCL/gelatin/PPy/graphene scaffold and PCL/PGS/PPy/graphene scaffold, ePTFE, and glass models. At each time point, blood treated with glass substance demonstrated a major difference in absorbance rate than PCL/gelatin/Ppy/graphene scaffold, PCL/PGS/PPy/graphene scaffold and ePTFE samples ($P < 0.05$) suggesting clot formation capability of glass compared to scaffold and ePTFE. The

results confirm that the electrospun PCL/gelatin/PPy/graphene scaffold, PCL/PGS/PPy/graphene scaffold and ePTFE samples have lower chance of thrombogenicity compare to glass samples.

3.6 Cell studies

Fibrous substance simulates the extracellular matrix (ECM) construction, accelerate cell proliferation and adhesion. Cellular interactions of the nanofibrous scaffolds were established by measuring two commonly known complementary assays; mitochondrial metabolic activity and cell viability. Fig. 8 demonstrates the cell viability assessments on PCL/gelatin/PPy/graphene and PCL/PGS/PPy/graphene fibrous scaffolds prepared using 3 wt.% graphene. Figure 8A-B shows SEM micrographs of fibroblast attachment on the scaffolds following 3 days. As it is shown, the scaffolds have maintained cell adhesion and multiplying. Interestingly, at day 7 (Fig. 8B), the scaffolds are intact and a greater area is covered with the cells. This suggests that the fibrous structure greatly supports the cell adhesion and proliferation. Furthermore, the MTT results confirms that the scaffolds are non-cytotoxic, support cell proliferation and do not inhibit cell growth.

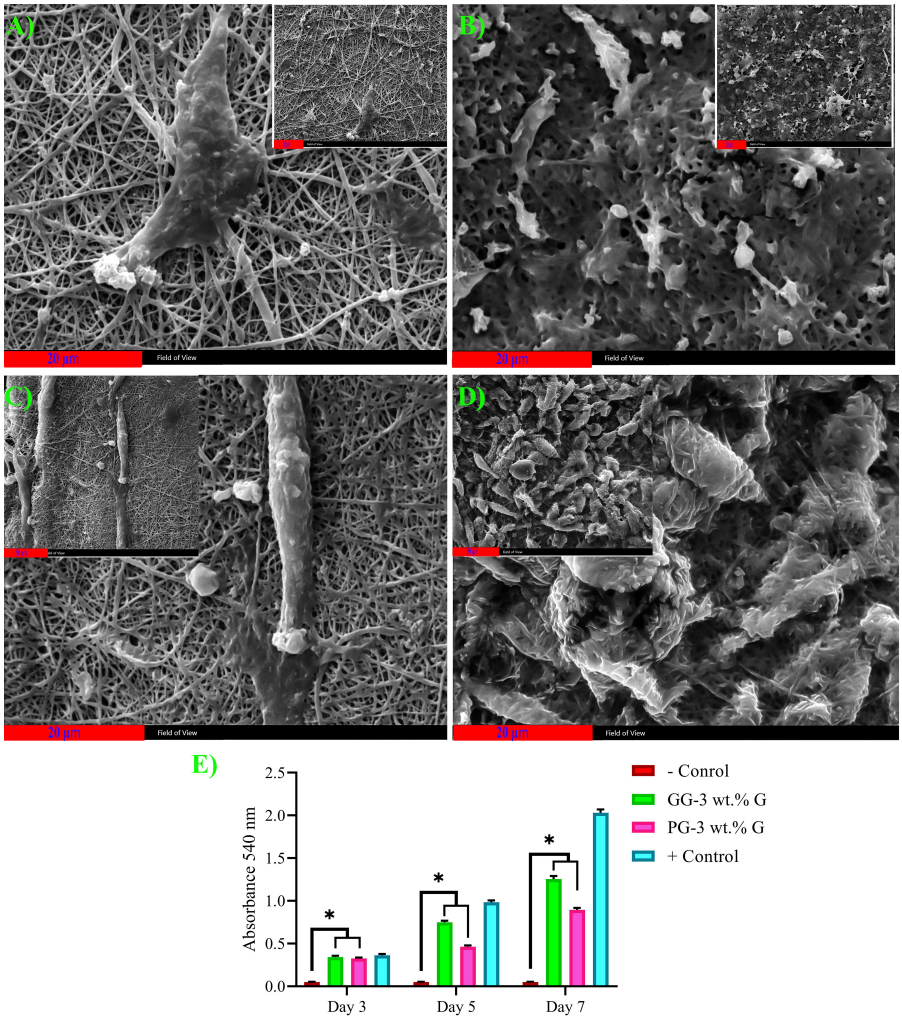

Figure 8. SEM images of human fibroblast cells on fibrous mat for PCL/gelatin/PPy/graphene blend following A) 3 and B) 7 days in culture and for PCL/PGS/PPy/graphene blend C) 3 and D) 7 days in culture. E) MTT cell viability assay of human fibroblast cultured on both blends. Scale bar: 20μm. Error bars indicate standard error of the means, asterisks mark significance levels of $p < 0.05$ (*).

4 Conclusion

In this study, a highly tunable nanofibrous structure suitable for conductive-tissue engineering applications was developed. The physical, chemical, mechanical, blood compatibility, and biological properties of two individual polymeric systems PCL/gelatin/PPy/graphene and PCL/PGS/PPy/graphene were fully evaluated. 3 wt.% graphene scaffolds showed superior overall mechanical strength, great electrical

conductivity and excellent hemocompatibility and biocompatibility. Overall, the results demonstrated remarkable tunable properties that can be controlled through the amount of graphene within the structure to mimic the native tissue properties.

Conflict of Interest:

The authors declare no conflict of interest.

Acknowledgement

We are immensely grateful to Iran's National Science Foundation for their financial supports (Grant Number 99012469).

References

(1) Wang, J.; Zhu, Y.-Q.; Wang, Y.; Xu, H.-G.; Xu, W.-J.; Wang, Y.-X.; Cheng, X.-Q.; Quan, Q.; Hu, Y.-Q.; Lu, C.-F.; Zhao, Y.-X.; Jiang, W.; Liu, C.; Xiao, L.; Lu, W.; Zhu, C.; Wang, A.-Y. A Novel Tissue Engineered Nerve Graft Constructed with Autologous Vein and Nerve Microtissue Repairs a Long-Segment Sciatic Nerve Defect. *Neural Regen. Res.* **2021**, *16* (1), 143. https://doi.org/10.4103/1673-5374.286977.

(2) Kornfeld, T.; Vogt, P. M.; Radtke, C. Nerve Grafting for Peripheral Nerve Injuries with Extended Defect Sizes. *Wiener Medizinische Wochenschrift* **2018**, *169* (9), 240–251. https://doi.org/10.1007/s10354-018-0675-6.

(3) Safa, B.; Buncke, G. Autograft Substitutes. Conduits and Processed Nerve Allografts. *Hand Clinics*. W.B. Saunders May 1, 2016, pp 127–140. https://doi.org/10.1016/j.hcl.2015.12.012.

(4) Patel, M.; Min, J. H.; Hong, M. H.; Lee, H. J.; Kang, S.; Yi, S.; Koh, W. G. Culture of Neural Stem Cells on Conductive and Microgrooved Polymeric Scaffolds Fabricated via Electrospun Fiberlate Lithography. *Biomed. Mater.* **2020**, *15* (4), 045007. https://doi.org/10.1088/1748-605X/ab763b.

(5) Vijayan, R.; Ghazinezami, A.; Taklimi, S. R.; Khan, M. Y.; Askari, D. The Geometrical Advantages of Helical Carbon Nanotubes for High-Performance Multifunctional Polymeric Nanocomposites. *Compos. Part B Eng.* **2019**, *156*, 28–42. https://doi.org/10.1016/j.compositesb.2018.08.035.

(6) Cleeton, C.; Keirouz, A.; Chen, X.; Radacsi, N. Electrospun Nanofibers for Drug Delivery and Biosensing. *ACS Biomater. Sci. Eng.* **2019**, *5* (9), 4183–4205. https://doi.org/10.1021/acsbiomaterials.9b00853.

(7) Xiao, P.; Qi, P.; Chen, J.; Song, Z.; Wang, Y.; He, H.; Tang, X.; Wang, P. The Effect of Polymer Blends on Initial Release Regulation and in Vitro-in Vivo Relationship of Peptides Loaded PLGA-Hydrogel Microspheres. *Int. J. Pharm.* **2020**, *591*, 119964. https://doi.org/10.1016/j.ijpharm.2020.119964.

(8) Gangrade, A.; Mandal, B. B. Injectable Carbon Nanotube Impregnated Silk Based Multifunctional Hydrogel for Localized Targeted and On-Demand Anticancer Drug Delivery. *ACS Biomater. Sci. Eng.* **2019**, *5* (5), 2365–2381. https://doi.org/10.1021/acsbiomaterials.9b00416.

(9) Brako, F.; Raimi-Abraham, B.; Mahalingam, S.; Craig, D. Q. M.; Edirisinghe, M. Making Nanofibres of Mucoadhesive Polymer Blends for Vaginal Therapies. *Eur. Polym. J.* **2015**, *70*, 186–196. https://doi.org/10.1016/j.eurpolymj.2015.07.006.

(10) Bochicchio, B.; Barbaro, K.; De Bonis, A.; Rau, J. V.; Pepe, A. Electrospun Poly(<scp>d,L</Scp> -lactide)/Gelatin/Glass-ceramics Tricomponent Nanofibrous Scaffold for Bone Tissue Engineering. *J. Biomed. Mater. Res. Part A* **2020**, *108* (5), 1064–1076. https://doi.org/10.1002/jbm.a.36882.

(11) Zhu, J.; Chen, D.; Du, J.; Chen, X.; Wang, J.; Zhang, H.; Chen, S.; Wu, J.; Zhu, T.; Mo, X. Mechanical Matching Nanofibrous Vascular Scaffold with Effective Anticoagulation for Vascular Tissue Engineering. *Compos. Part B Eng.* **2020**, *186*, 107788. https://doi.org/10.1016/j.compositesb.2020.107788.

(12) Askarzadeh, N.; Nazarpak, M. H.; Mansoori, K.; Farokhi, M.; Gholami, M.; Mohammadi, J.; Mottaghitalab, F. Bilayer Cylindrical Conduit Consisting of Electrospun Polycaprolactone Nanofibers and DSC Cross-Linked Sodium Alginate Hydrogel to Bridge Peripheral Nerve Gaps. *Macromol. Biosci.* **2020**, *20* (9), 2000149.

https://doi.org/10.1002/mabi.202000149.

(13) Hong, S.; Kim, G. H. Electrospun Polycaprolactone/Silk Fibroin/Small Intestine Submucosa Composites for Biomedical Applications. *Macromol. Mater. Eng.* **2010**, *295* (6), 529–534. https://doi.org/10.1002/mame.201000051.

(14) Bayram, C.; Jiang, X.; Gultekinoglu, M.; Ozturk, S.; Ulubayram, K.; Edirisinghe, M. Biofabrication of Gelatin Tissue Scaffolds with Uniform Pore Size via Microbubble Assembly. *Macromol. Mater. Eng.* **2019**, *304* (11), 1900394. https://doi.org/10.1002/mame.201900394.

(15) Wang, J.; Tian, L.; He, L.; Chen, N.; Ramakrishna, S.; So, K.-F.; Mo, X. Lycium Barbarum Polysaccharide Encapsulated Poly Lactic-Co-Glycolic Acid Nanofibers: Cost Effective Herbal Medicine for Potential Application in Peripheral Nerve Tissue Engineering. *Sci. Rep.* **2018**, *8* (1), 8669. https://doi.org/10.1038/s41598-018-26837-z.

(16) Hu, J.; Kai, D.; Ye, H.; Tian, L.; Ding, X.; Ramakrishna, S.; Loh, X. J. Electrospinning of Poly(Glycerol Sebacate)-Based Nanofibers for Nerve Tissue Engineering. *Mater. Sci. Eng. C* **2017**, *70*, 1089–1094. https://doi.org/10.1016/j.msec.2016.03.035.

(17) Flaig, F.; Ragot, H.; Simon, A.; Revet, G.; Kitsara, M.; Kitasato, L.; Hébraud, A.; Agbulut, O.; Schlatter, G. Design of Functional Electrospun Scaffolds Based on Poly(Glycerol Sebacate) Elastomer and Poly(Lactic Acid) for Cardiac Tissue Engineering. *ACS Biomater. Sci. Eng.* **2020**, *6* (4), 2388–2400. https://doi.org/10.1021/acsbiomaterials.0c00243.

(18) Kenar, H.; Kose, G. T.; Toner, M.; Kaplan, D. L.; Hasirci, V. A 3D Aligned Microfibrous Myocardial Tissue Construct Cultured under Transient Perfusion. *Biomaterials* **2011**, *32* (23), 5320–5329. https://doi.org/10.1016/j.biomaterials.2011.04.025.

(19) Ravichandran, R.; Venugopal, J. R.; Sundarrajan, S.; Mukherjee, S.; Sridhar, R.; Ramakrishna, S. Minimally Invasive Injectable Short Nanofibers of Poly(Glycerol Sebacate) for Cardiac Tissue Engineering. *Nanotechnology* **2012**, *23* (38), 385102. https://doi.org/10.1088/0957-4484/23/38/385102.

(20) Li, W.-J.; Cooper, J. A.; Mauck, R. L.; Tuan, R. S. Fabrication and Characterization of Six Electrospun Poly(α-Hydroxy Ester)-Based Fibrous Scaffolds for Tissue

Engineering Applications. *Acta Biomater.* **2006**, *2* (4), 377–385. https://doi.org/https://doi.org/10.1016/j.actbio.2006.02.005.

(21) Akşit, N. N.; Gürdap, S.; İşoğlu, S. D.; İşoğlu, İ. A. Preparation of Antibacterial Electrospun Poly(D, L-Lactide-Co-Glycolide)/Gelatin Blend Membranes Containing Hypericum Capitatum Var. Capitatum. *Int. J. Polym. Mater. Polym. Biomater.* **2020**. https://doi.org/10.1080/00914037.2020.1765354.

(22) Samadian, H.; Ehterami, A.; Sarrafzadeh, A.; Khastar, H.; Nikbakht, M.; Rezaei, A.; Chegini, L.; Salehi, M. Sophisticated Polycaprolactone/Gelatin Nanofibrous Nerve Guided Conduit Containing Platelet-Rich Plasma and Citicoline for Peripheral Nerve Regeneration: In Vitro and in Vivo Study. *Int. J. Biol. Macromol.* **2020**, *150*, 380–388. https://doi.org/https://doi.org/10.1016/j.ijbiomac.2020.02.102.

(23) Kireev, D.; Offenhäusser, A. Graphene & Two-Dimensional Devices for Bioelectronics and Neuroprosthetics. *2D Materials*. IOP Publishing Ltd September 7, 2018, p 042004. https://doi.org/10.1088/2053-1583/aad988.

(24) Wang, J.; Zheng, W.; Chen, L.; Zhu, T.; Shen, W.; Fan, C.; Wang, H.; Mo, X. Enhancement of Schwann Cells Function Using Graphene-Oxide-Modified Nanofiber Scaffolds for Peripheral Nerve Regeneration. *ACS Biomater. Sci. Eng.* **2019**. https://doi.org/10.1021/acsbiomaterials.8b01564.

(25) Kabiri, M.; Oraee-Yazdani, S.; Dodel, M.; Hanaee-Ahvaz, H.; Soudi, S.; Seyedjafari, E.; Salehi, M.; Soleimani, M. Cytocompatibility of a Conductive Nanofibrous Carbon Nanotube/Poly (L-Lactic Acid) Composite Scaffold Intended for Nerve Tissue Engineering. *EXCLI J.* **2015**, *14*, 851–860. https://doi.org/10.17179/excli2015-282.

(26) Cooper, A.; Bhattarai, N.; Zhang, M. Fabrication and Cellular Compatibility of Aligned Chitosan-PCL Fibers for Nerve Tissue Regeneration. *Carbohydr. Polym.* **2011**, *85* (1), 149–156. https://doi.org/10.1016/j.carbpol.2011.02.008.

(27) Wang, S.; Guan, S.; Zhu, Z.; Li, W.; Liu, T.; Ma, X. Hyaluronic Acid Doped-Poly(3,4-Ethylenedioxythiophene)/Chitosan/Gelatin (PEDOT-HA/Cs/Gel) Porous Conductive Scaffold for Nerve Regeneration. *Mater. Sci. Eng. C* **2017**, *71*, 308–316. https://doi.org/10.1016/j.msec.2016.10.029.

(28) Talebi, A.; Labbaf, S.; Karimzadeh, F.; Masaeli, E.; Nasr Esfahani, M.-H.

Electroconductive Graphene-Containing Polymeric Patch: A Promising Platform for Future Cardiac Repair. *ACS Biomater. Sci. Eng.* **2020**, acsbiomaterials.0c00266. https://doi.org/10.1021/acsbiomaterials.0c00266.

(29) Talebi, A.; Labbaf, S.; Karimzadeh, F. A Conductive Film of Chitosan-Polycaprolcatone-Polypyrrole with Potential in Heart Patch Application. *Polym. Test.* **2019**, *75*. https://doi.org/10.1016/j.polymertesting.2019.02.029.

(30) Kharazi, A. Z.; Atari, M.; Vatankhah, E.; Javanmard, S. H. A Nanofibrous Bilayered Scaffold for Tissue Engineering of Small-Diameter Blood Vessels. *Polym. Adv. Technol.* **2018**, *29* (12), 3151–3158. https://doi.org/10.1002/pat.4437.

(31) Jiang, L.; Jun, H.; Hoh, Y.; Lim, J.; … D. L.-S. and A. B.; 2005, U. Sensing Characteristics of Polypyrrole–Poly (Vinyl Alcohol) Methanol Sensors Prepared by in Situ Vapor State Polymerization. *Elsevier*.

(32) Talebi, A.; Labbaf, S.; Karimzadeh, F. Polycaprolactone-chitosan-polypyrrole Conductive Biocomposite Nanofibrous Scaffold for Biomedical Applications. *Polym. Compos.* **2019**, pc.25395. https://doi.org/10.1002/pc.25395.

(33) Chiu, N.-F.; Fan, S.-Y.; Yang, C.-D.; Huang, T.-Y. Carboxyl-Functionalized Graphene Oxide Composites as SPR Biosensors with Enhanced Sensitivity for Immunoaffinity Detection. *Biosens. Bioelectron.* **2017**, *89*, 370–376. https://doi.org/10.1016/J.BIOS.2016.06.073.

(34) Wang, X.; Ding, B.; Li, B. Biomimetic Electrospun Nanofibrous Structures for Tissue Engineering. *Mater. Today* **2013**, *16* (6), 229–241. https://doi.org/10.1016/J.MATTOD.2013.06.005.

(35) Saberi, A.; Jabbari, F.; Zarrintaj, P.; Saeb, M. R.; Mozafari, M. Electrically Conductive Materials: Opportunities and Challenges in Tissue Engineering. *Biomolecules* **2019**, *9* (9). https://doi.org/10.3390/biom9090448.

(36) Ghasemi-Mobarakeh, L.; Prabhakaran, M. P.; Morshed, M.; Nasr-Esfahani, M. H.; Ramakrishna, S. Electrospun Poly(ε-Caprolactone)/Gelatin Nanofibrous Scaffolds for Nerve Tissue Engineering. *Biomaterials* **2008**, *29* (34), 4532–4539. https://doi.org/10.1016/j.biomaterials.2008.08.007.

(37) Baniasadi, H.; Ramazani S.A., A.; Mashayekhan, S. Fabrication and Characterization

of Conductive Chitosan/Gelatin-Based Scaffolds for Nerve Tissue Engineering. *Int. J. Biol. Macromol.* **2015**, *74*, 360–366. https://doi.org/https://doi.org/10.1016/j.ijbiomac.2014.12.014.

(38) Zhou, J.-F.; Wang, Y.-G.; Cheng, L.; Wu, Z.; Sun, X.-D.; Peng, J. Preparation of Polypyrrole-Embedded Electrospun Poly(Lactic Acid) Nanofibrous Scaffolds for Nerve Tissue Engineering. *Neural Regen. Res.* **2016**, *11* (10), 1644–1652. https://doi.org/10.4103/1673-5374.193245.

(39) Soltani, S.; Ebrahimian-Hosseinabadi, M.; Zargar Kharazi, A. Chitosan/Graphene and Poly(D, L-Lactic-Co-Glycolic Acid)/Graphene Nano-Composites for Nerve Tissue Engineering. *Tissue Eng. Regen. Med.* **2016**, *13* (6), 684–690. https://doi.org/10.1007/s13770-016-9130-1.

(40) Cheng, S.; Bilston, L. E. Unconfined Compression of White Matter. *J. Biomech.* **2007**, *40* (1), 117–124. https://doi.org/https://doi.org/10.1016/j.jbiomech.2005.11.004.

(41) Hung, T. K.; Chang, G. L. Biomechaniol and Neurological Response of the Spinal Cord of a Puppy to Uniaxial Tension. *J. Biomech. Eng.* **1981**, *103* (1), 43–47. https://doi.org/10.1115/1.3138244.

(42) Hung, T.-K.; Chang, G.-L.; Chang, J.-L.; Albin, M. S. Stress-Strain Relationship and Neurological Sequelae of Uniaxial Elongation of the Spinal Cord of Cats. *Surg. Neurol.* **1981**, *15* (6), 471–476. https://doi.org/10.1016/S0090-3019(81)80043-2.

(43) Ebrahimi, A. P. Mechanical Properties of Normal and Diseased Cerebrovascular System. *J. Vasc. Interv. Neurol.* **2009**, *2* (2), 155–162.

(44) Mao, N.; Russell, S. J. A Framework for Determining the Bonding Intensity in Hydroentangled Nonwoven Fabrics. *Compos. Sci. Technol.* **2006**, *66* (1), 80–91. https://doi.org/10.1016/j.compscitech.2005.05.030.

(45) Liau, B.; Zhang, D.; Bursac, N. Functional Cardiac Tissue Engineering. *Regen. Med.* **2012**, *7* (2), 187–206. https://doi.org/10.2217/rme.11.122.

(46) Ding, X.; Chen, Y.; Chao, C. A.; Wu, Y.; Wang, Y. Control the Mechanical Properties and Degradation of Poly(Glycerol Sebacate) by Substitution of the Hydroxyl Groups with Palmitates. *Macromol. Biosci.* **2020**, *20* (9), 2000101. https://doi.org/10.1002/mabi.202000101.

(47) Liang, S. L.; Yang, X. Y.; Fang, X. Y.; Cook, W. D.; Thouas, G. A.; Chen, Q. Z. In Vitro Enzymatic Degradation of Poly (Glycerol Sebacate)-Based Materials. *Biomaterials* **2011**, *32* (33), 8486–8496. https://doi.org/10.1016/j.biomaterials.2011.07.080.

(48) Gorbet, M. B.; Sefton, M. V. Review: Biomaterial-Associated Thrombosis: Roles of Coagulation Factors, Complement, Platelets and Leukocytes. *Biomater. Silver Jubil. Compend.* **2004**, 219–241. https://doi.org/10.1016/B978-008045154-1.50025-3.

(49) Menzies, K. L.; Jones, L. The Impact of Contact Angle on the Biocompatibility of Biomaterials. *Optom. Vis. Sci.* **2010**, 1. https://doi.org/10.1097/OPX.0b013e3181da863e.

(50) Singhal, J. P.; Ray, A. R. Synthesis of Blood Compatible Polyamide Block Copolymers. *Biomaterials* **2002**, *23* (4), 1139–1145. https://doi.org/10.1016/S0142-9612(01)00228-9.

(51) Tu, Y.; Lv, M.; Xiu, P.; Huynh, T.; Zhang, M.; Castelli, M.; Liu, Z.; Huang, Q.; Fan, C.; Fang, H.; Zhou, R. Destructive Extraction of Phospholipids from Escherichia Coli Membranes by Graphene Nanosheets. *Nat. Nanotechnol.* **2013**, *8* (8), 594–601. https://doi.org/10.1038/nnano.2013.125.

(52) Cai, B.; Hu, K.; Li, C.; Jin, J.; Hu, Y. Applied Surface Science Bovine Serum Albumin Bioconjugated Graphene Oxide : Red Blood Cell Adhesion and Hemolysis Studied by QCM-D. *Appl. Surf. Sci.* **2015**, *356*, 844–851. https://doi.org/10.1016/j.apsusc.2015.08.178.

(53) Liu, H. Y.; Du, L.; Zhao, Y. T.; Tian, W. Q. In Vitro Hemocompatibility and Cytotoxicity Evaluation of Halloysite Nanotubes for Biomedical Application. *J. Nanomater.* **2015**. https://doi.org/10.1155/2015/685323.